

# Driftless 3-D Attitude Determination and Positioning of Mobile Robots By Integration of IMU With Two RTK GPSs

Farhad Aghili, *Senior Member, IEEE*, and Alessio Salerno, *Member, IEEE*

**Abstract**—This paper focuses on the integration of inertial measurement unit (IMU) with two real-time kinematic global positioning system (GPS) units in an adaptive Kalman filter (KF) for driftless estimation of a vehicle's attitude and position in 3-D. The observability analysis reveals that 1) integration of a single GPS with IMU does not constitute an observable system; and 2) integration of two GPS units with IMU results in a locally observable system provided that the line connecting two GPS antennas is not parallel with the vector of the measured acceleration, i.e., the sum of inertial and gravitational accelerations. The latter case makes it possible to compensate the error in the estimated orientation due to gyro drift and its bias without needing additional instrument for absolute orientation measurements, e.g., magnetic compass. Moreover, in order to cope with the fact that GPS systems sometimes lose their signal and receive inaccurate position data, the self-tuning filter estimates the covariance matrix associated with the GPS measurement noise. This allows the KF to incorporate GPS measurements in the data fusion process heavily only when the information received by GPS becomes reliably available. Finally, test results obtained from a mobile robot moving across uneven terrain demonstrate driftless 3-D pose estimation.

**Index Terms**—Attitude determination, global positioning system, global positioning system-inertial measurement unit (GPS-IMU) integration, inertial measurement unit, Kalman filtering, localization of mobile robots, navigation of vehicles, pose estimation, real-time kinematic global positioning system (RTK GPS).

## I. INTRODUCTION

BOOTH position and attitude determination of a mobile robot are necessary for navigation, guidance, and steering control of a mobile robot. *Dead reckoning* using vehicle kinematic model and incremental measurement of wheel encoders is the common technique to determine the position and orientation of mobile robots for indoors applications [1]. However, the application of these techniques for localization of outdoor robots is limited, particularly when the robot has to traverse an uneven terrain or loose soils. This is because wheel slippage and wheel imperfection cause quick accumulation of the position and attitude errors [2]. Other research utilizes inertial measure-

ment unit (IMU) and wheel encoders to obtain close estimate of robot position [3]–[9]. The problem with inertial systems, however, is that they require additional information about absolute position and orientation to overcome long-term drift [10]. Yi *et al.* [9] proposed integration of the kinematic relationship between wheel slip and instantaneous rotation center of skid-steered mobile robots with onboard IMU and wheel encoder to improve motion-estimation accuracy in 2-D environment.

In essence, to measure the pose of a vehicle with high bandwidth and long-term accuracy and stability usually involves data fusion of different sensors because there is no single sensor to satisfy both requirements. In this respect, global positioning system (GPS) and IMU are considered complementary positioning systems: GPS systems provide low update rate, but they have the advantage of long-term position accuracy. Conversely, IMU systems provide high-bandwidth position information, while they are characterized by long-term drift. Additionally, integration of the inertial data continuously provides pose estimation even when the GPS systems lose their signal and receive inaccurate position data namely due to obstruction. Since no wheel odometry is used in this localization method, one can envisage the application of this localization method to humanoid [11] and legged robots as well as aerial vehicles [12].

Nowadays, differential GPSs to centimeter-level accuracy are commercially available making them attractive for localization, guidance, and control of outdoor mobile robots [13]–[26]. Improving the accuracy of localization systems using real-time kinematic (RTK) GPS in the presence of GPS latency was addressed in [13]. A localization algorithm based on Kalman filtering to fuse data from a single GPS and several other sensors and map-based data was presented in [14]. The onboard sensory system includes wheel encodes, inertial navigation system (INS), a laser scanner for relative position measurements, and a GPS antenna for absolute position measurements. An autonomous mobile robot using GPS and photosensors was presented in [16]. The feasibility of a low-order vehicle positioning system functioning under an urban environment was investigated in [17]. This positioning system is based on integration of INS with a single GPS unit that can provide the vehicle heading angle based on the Doppler effect. Low and Wang proposed a pose estimator using a single RTK GPS and inertial sensors for motion estimation of a wheeled mobile robot in 2-D environment to deal with skidding and slipping problem [19], [20]. However, this sensor fusion method relies on additional instrument for absolute orientation measurements. Similarly, a magnetic compass was incorporated in data fusion of a microelectromechanical

Manuscript received April 20, 2011; revised June 8, 2011; accepted June 26, 2011. Date of publication August 4, 2011; date of current version September 12, 2012. Recommended by Technical Editor G. Liu.

F. Aghili is with the Canadian Space Agency, Saint-Hubert, QC J3Y 8Y9, Canada (e-mail: farhad.aghili@asc-csa.gc.ca).

A. Salerno was with the Canadian Space Agency, Saint-Hubert, QC J3Y 8Y9, Canada. He is now with Pratt & Whitney Canada, Longueuil, QC J4G 1A1, Canada (e-mail: alessio.salerno@asc-csa.gc.ca).

Color versions of one or more of the figures in this paper are available online at <http://ieeexplore.ieee.org>.

Digital Object Identifier 10.1109/TMECH.2011.2161485

system-IMU/GPS integrated navigation system proposed in [27] in order to make the heading angle observable. A decentralized data fusion algorithm is presented [24] for simultaneous position estimation of a land vehicle and building the map of the environment by incorporating data from inertial sensor, GPS, laser scanner, and the wheel and steering encoders. The majority of the aforementioned techniques for integration of IMU with GPS utilize a single GPS antennas, and hence, they require additional instrument for absolute orientation measurement, e.g., magnetic compass or laser scanner. Although there are GPS devices that can provide vehicle heading angles based on Doppler effect, the accuracy of the angle measurement drops significantly at low speeds and it does not work at zero speed.

This paper presents fusing data from IMU and two RTK GPS units in an adaptive Kalman filter (KF) to estimate the attitude, position, and velocity of a vehicle in 3-D. Observability analysis of GPS/IMU integration system is investigated in this paper. The results show that the states of the system are observable provided that at least two GPS antennas are utilized and that the line connecting two GPS antennas is not parallel to the acceleration measurement vector. In other words, a conventional GPS/IMU integration scheme using one GPS unit is not observable whereas the observability of the integration system using two GPS units can be ensured at the cost of adding an extra GPS unit to the integration system and that constitutes the main contribution of this paper. Moreover, RTK GPS devices notoriously suffer from signal robustness issue as their signal can be easily disturbed by many factors such as satellite geometry, atmospheric condition, and shadow. To deal with the uncertain GPS noise problem, the covariance matrix of the GPS noises is estimated in real time so that the KF filter incorporates GPS information heavily in the data fusion process only when the GPS measurements become reliably available. Tests have been conducted on the Canadian Space Agency (CSA) *red rover* for assessing the performance of our pose estimator. This paper is organized as follows. Section II describes the observation and process models pertaining to the positioning system consisting of two GPSs and an IMU. Observability analysis of such a positioning system is given in Section II-B. In Section III, the fusing of accelerometer, rate gyro, and GPS information in a self-tuning adaptive KF is developed. Finally, the experimental results are reported in Section IV.

## II. MODELING AND ANALYSIS

Fig. 1 schematically illustrates a vehicle as a rigid body to which two differential GPS antennas and an IMU device are attached. Coordinate frame  $\{\mathcal{A}\}$  is an inertial frame while  $\{\mathcal{B}\}$  is a vehicle-fixed (body frame) coordinate system. The origin of frame  $\{\mathcal{A}\}$  coincides with that of the GPS base antenna, i.e., the vehicle GPS measurements are expressed in  $\{\mathcal{A}\}$ . Without loss of generality, we assume that the vehicle body frame  $\{\mathcal{B}\}$  coincides with the IMU coordinate frame, i.e., the IMU measurements are expressed in  $\{\mathcal{B}\}$ . The orientation of  $\{\mathcal{B}\}$  with respect to  $\{\mathcal{A}\}$  is represented by the unit quaternion  $\mathbf{q} = [\mathbf{q}_v^T \ q_o]^T$ , where subscripts  $v$  and  $o$  denote the vector and scalar parts of the quaternion, respectively. The rotation matrix  $\mathbf{A}$  representing

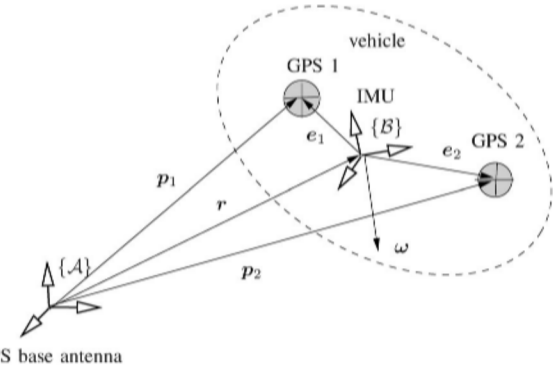


Fig. 1. Two GPS antennas and an IMU attached on a vehicle body.

the rotation of frame  $\{\mathcal{B}\}$  with respect to frame  $\{\mathcal{A}\}$  is related to the corresponding quaternion  $\mathbf{q}$  by

$$\mathbf{A}(\mathbf{q}) = (2q_o^2 - 1)\mathbf{I}_3 + 2\mathbf{q}_v[\mathbf{q}_v \times] + 2\mathbf{q}_v\mathbf{q}_v^T \quad (1)$$

where  $[\cdot \times]$  denotes the matrix form of the cross product and  $\mathbf{I}_n$  denotes the  $n \times n$  identity matrix. The quaternion product  $\otimes$  is defined as

$$\mathbf{q} \otimes = q_o \mathbf{I}_4 + \boldsymbol{\Omega}(\mathbf{q}_v) \quad \text{where} \quad \boldsymbol{\Omega}(\mathbf{q}_v) = \begin{bmatrix} -[\mathbf{q}_v \times] & \mathbf{q}_v \\ -\mathbf{q}_v^T & 0 \end{bmatrix}$$

so that  $\mathbf{q}_1 \otimes \mathbf{q}_2$  corresponds to rotation matrix  $\mathbf{A}(\mathbf{q}_2)\mathbf{A}(\mathbf{q}_1)$ .

### A. Observation and Process Models

This section first presents the measurement model, followed by the process model including the close forms of the state transition matrix and the discrete-time process noise needed for covariance propagation. The GPS measurements are directly included in the measurement equations, while the IMU outputs are treated as the time-varying inputs of the process system.

Assume that vector  $\mathbf{r}$  represents the location of the origin of frame  $\{\mathcal{B}\}$  that is expressed in coordinate frame  $\{\mathcal{A}\}$ , and  $\mathbf{p}_i$  is the output of the  $i$ th GPS measurement. Apparently, from Fig. 1, we have

$$\mathbf{p}_i = \mathbf{r} + \mathbf{A}(\mathbf{q})\mathbf{e}_i, \quad i = 1, 2 \quad (2)$$

where constant vectors  $\mathbf{e}_1$  and  $\mathbf{e}_2$  are the locations of the corresponding GPS antennas expressed in the IMU frame.

Let us define the state vector to be estimated by the extended KF (EKF) as  $\mathbf{x} = [\mathbf{q}_v^T \ \mathbf{r}^T \ \dot{\mathbf{r}}^T \ \mathbf{b}^T]^T$ , where vector  $\mathbf{b}$  is the gyro bias. Then, one can write the observation vector as a nonlinear function of the state

$$\mathbf{z} = \mathbf{h}(\mathbf{x}) + \mathbf{v}$$

where

$$\mathbf{z} = \begin{bmatrix} \mathbf{p}_1 \\ \mathbf{p}_2 \end{bmatrix}, \quad \mathbf{h}(\mathbf{x}) = \begin{bmatrix} \mathbf{r} + \mathbf{A}(\mathbf{q})\mathbf{e}_1 \\ \mathbf{r} + \mathbf{A}(\mathbf{q})\mathbf{e}_2 \end{bmatrix} \quad (3)$$

and  $\mathbf{v}$  represents the GPS measurement noise, which is assumed random walk with covariance  $\mathbf{r} = E[\mathbf{v}\mathbf{v}^T]$ .

To linearize the observation vector  $\mathbf{h}(\mathbf{x})$  one needs to derive the sensitivity of the nonlinear observation vector with respect

to the system state vector. Consider small variation of the quaternion from its estimation  $\hat{\mathbf{q}}$  as

$$\delta\mathbf{q} = \mathbf{q} \otimes \hat{\mathbf{q}}^* \quad (4)$$

where  $\hat{\mathbf{q}}^*$  is the inverse of quaternion  $\hat{\mathbf{q}}$ , i.e.,  $\hat{\mathbf{q}}^* \otimes \hat{\mathbf{q}} = [0 \ 0 \ 0 \ 1]^T$ . In other words, identity  $\mathbf{A}(\mathbf{q}^*) \equiv [\mathbf{A}(\mathbf{q})]^T$  is in order for all quaternion  $\mathbf{q}$ . Notice that in the following, the “hat” sign depicts the estimation of a variable. Now, by virtue of  $\mathbf{A}(\mathbf{q}) = \mathbf{A}(\delta\mathbf{q} \otimes \hat{\mathbf{q}})$ , one can compute the observation vector (3) in terms of the perturbation  $\delta\mathbf{q}$ . Using the first-order approximation of nonlinear matrix function  $\mathbf{A}(\delta\mathbf{q})$  from expression (1) by assuming a small rotation  $\delta\mathbf{q}$ , i.e.,  $\|\delta\mathbf{q}_v\| \ll 1$  and  $\delta q_0 \approx 1$ , we will have

$$\mathbf{A}(\delta\mathbf{q}) = \mathbf{I}_3 + 2[\delta\mathbf{q}_v \times] + \text{HOT}. \quad (5)$$

Thus, the sensitivity matrix can be written as

$$\mathbf{h} = \frac{\partial \mathbf{h}}{\partial \mathbf{x}} \Big|_{\mathbf{x}=\hat{\mathbf{x}}} = \begin{bmatrix} -2\hat{\mathbf{A}}[\mathbf{e}_1 \times] & \mathbf{I}_3 & \mathbf{0}_3 & \mathbf{0}_3 \\ -2\hat{\mathbf{A}}[\mathbf{e}_2 \times] & \mathbf{I}_3 & \mathbf{0}_3 & \mathbf{0}_3 \end{bmatrix} \quad (6)$$

where  $\hat{\mathbf{A}} = \mathbf{A}(\hat{\mathbf{q}})$ .

Denoting the angular velocity of the vehicle by  $\boldsymbol{\omega}$ , the relation between the time derivative of the quaternion and the angular velocity can be readily expressed by

$$\dot{\mathbf{q}} = \frac{1}{2}\boldsymbol{\Omega}(\boldsymbol{\omega})\mathbf{q}. \quad (7)$$

The angular rate is related to the rate gyro measurement by

$$\boldsymbol{\omega} = \mathbf{u}_g + \mathbf{b} + \mathbf{w}_g$$

where  $\mathbf{u}_g$  is the gyro output,  $\mathbf{b}$  is the gyro bias vector, and  $\mathbf{w}_g$  is the angular random walk noise of the gyro rate with covariance  $E[\mathbf{w}_g \mathbf{w}_g^T] = \sigma_g^2 \mathbf{I}_3$ . The time derivative of gyro bias is traditionally modeled with random walk model [28], [29] according to

$$\dot{\mathbf{b}} = \mathbf{w}_b \quad (8)$$

where  $\mathbf{w}_b$  is the rate random walk noise with covariance  $E[\mathbf{w}_b \mathbf{w}_b^T] = \sigma_b^2 \mathbf{I}_3$ .

A measurement of the linear acceleration of the vehicle is provided by an accelerometer. We assume that the deterministic error sources of the accelerometer unit, which include scale factor and offset, are compensated. The error can be compensated either internally by its signal processor or externally by a calibration procedure [30]. However, accelerometers cannot distinguish between the acceleration of gravity and inertial acceleration. Therefore, the accelerometer output equation is represented by

$$\ddot{\mathbf{r}} = \mathbf{A}(\mathbf{q})(\mathbf{u}_a + \mathbf{w}_a) - \mathbf{g} \quad (9)$$

where  $\mathbf{u}_a$  is the acceleration output,  $\mathbf{w}_a$  is the accelerometer noise assumed to be random walk noise  $\mathbf{w}_a$  with covariance  $E[\mathbf{w}_a \mathbf{w}_a^T] = \sigma_a^2 \mathbf{I}_3$ , and  $\mathbf{g}$  is the constant gravity vector. Therefore, in view of (7), (8), and (9), the process dynamics can be described by

$$\dot{\mathbf{x}} = \mathbf{f}(\mathbf{x}, \mathbf{u}, \mathbf{w}) \quad (10)$$

where vector  $\mathbf{u} = [\mathbf{u}_g^T \ \mathbf{u}_a^T]^T$  contains the IMU outputs, vector  $\mathbf{w} = [\mathbf{w}_g^T \ \mathbf{w}_a^T \ \mathbf{w}_b^T]^T$  contains the entire process noise

$$\mathbf{f}(\mathbf{x}, \mathbf{u}, \mathbf{w}) = \begin{bmatrix} \frac{1}{2}\text{vec}[\boldsymbol{\Omega}(\mathbf{u}_g + \mathbf{b} + \mathbf{w}_g)\mathbf{q}] \\ \dot{\mathbf{r}} \\ \mathbf{A}(\mathbf{q})(\mathbf{u}_a + \mathbf{w}_a) - \mathbf{g} \\ \mathbf{w}_b \end{bmatrix}$$

and  $\text{vec}(\cdot)$  returns the vector part of a quaternion.

Although the states can be propagated by solving the nonlinear dynamics equations (10), the state transition matrix of the linearized dynamics equations will be also needed to be used for covariance propagation of the KF. Adopting a linearization technique similar to [28], [29], one can linearize (7) about the quaternion estimation  $\hat{\mathbf{q}}$  and  $\hat{\boldsymbol{\omega}} = \hat{\mathbf{u}}_g + \hat{\mathbf{b}}$  to obtain

$$\frac{d}{dt}\delta\mathbf{q}_v = -\hat{\boldsymbol{\omega}} \times \delta\mathbf{q}_v + \frac{1}{2}\delta\mathbf{b} + \frac{1}{2}\mathbf{w}_g \quad (11a)$$

$$\frac{d}{dt}\delta q_o = 0. \quad (11b)$$

Since  $\delta q_o$  is not an independent variable and it has variations of only the second order, its time derivative can be ignored, as suggested in [28].

Similarly, the equation of translational motion (9) can be linearized about the acceleration estimation,  $\hat{\mathbf{a}} = \hat{\mathbf{u}}_a$ , and  $\hat{\mathbf{q}}$  using the first-order approximation (5) as

$$\begin{aligned} \delta\ddot{\mathbf{r}} &= \mathbf{A}(\delta\mathbf{q} \otimes \hat{\mathbf{q}})(\hat{\mathbf{a}} + \mathbf{w}_a) - \mathbf{A}(\hat{\mathbf{q}})\hat{\mathbf{a}} \\ &\approx -2\hat{\mathbf{A}}[\hat{\mathbf{a}} \times]\delta\mathbf{q}_v + \hat{\mathbf{A}}\mathbf{w}_a. \end{aligned} \quad (12)$$

Thus, setting (8), (11a), and (12) in the state-space form, the linearized model of the continuous system can be derived as

$$\mathbf{F} = \frac{\partial \mathbf{f}}{\partial \mathbf{x}} \Big|_{\substack{\mathbf{x}=\hat{\mathbf{x}} \\ \mathbf{u}=\hat{\mathbf{u}}}} = \begin{bmatrix} -[\hat{\boldsymbol{\omega}} \times] & \mathbf{0}_3 & \mathbf{0}_3 & \frac{1}{2}\mathbf{I}_3 \\ \mathbf{0}_3 & \mathbf{0}_3 & \mathbf{I}_3 & \mathbf{0}_3 \\ -2\hat{\mathbf{A}}[\hat{\mathbf{a}} \times] & \mathbf{0}_3 & \mathbf{0}_3 & \mathbf{0}_3 \\ \mathbf{0}_3 & \mathbf{0}_3 & \mathbf{0}_3 & \mathbf{0}_3 \end{bmatrix} \quad (13a)$$

$$\mathbf{G} = \frac{\partial \mathbf{f}}{\partial \mathbf{w}} \Big|_{\mathbf{x}=\hat{\mathbf{x}}} = \begin{bmatrix} \frac{1}{2}\mathbf{I}_3 & \mathbf{0}_3 & \mathbf{0}_3 \\ \mathbf{0}_3 & \mathbf{0}_3 & \mathbf{0}_3 \\ \mathbf{0}_3 & \hat{\mathbf{A}} & \mathbf{0}_3 \\ \mathbf{0}_3 & \mathbf{0}_3 & \mathbf{I}_3 \end{bmatrix}. \quad (13b)$$

### B. Observability Analysis

The KF built around a system whose states are not observable does not simply work [31]. Therefore, a successful use of Kalman filtering requires that the system be observable. A linear time-invariant systems is said to be *globally observable* if and only if its observability matrix is full rank. If a system is observable, the estimation error becomes only a function of the system noise, while the effect of the initial values of the states on the error will asymptotically vanish. In that case, the time-varying system (6) and (13a) can be replaced by a piecewise

constant system for observability analysis [32], [33]. The intuitive notion is that such a time-varying system can be effectively approximated by a piecewise constant system without loosing the characteristic behavior of the original system [32].

This section examines the observability of the IMU/GPS integration system for two cases: 1) two GPS units are incorporated in the sensor fusion; and 2) a single GPS unit is incorporated.

1) *Dual-GPS/IMU Integration*: The observability matrix associated with linearized system (13a) together with the observation model (6) is

$$\mathcal{O} = [\mathbf{H}^T \quad (\mathbf{H}\mathbf{F})^T \quad \cdots \quad (\mathbf{H}\mathbf{F}^{11})^T]^T. \quad (14)$$

The states of the system are assumed to be completely observable if and only if

$$\text{rank } \mathcal{O} = 12 \quad (15)$$

which is equivalent to  $\mathcal{O}$  having 12 independent rows. Now, let us construct the submatrices of the observability matrix  $\mathcal{O}$  from (6) and (13a) as

$$\mathbf{H}\mathbf{F} = \begin{bmatrix} 2\hat{\mathbf{A}}[\mathbf{e}_1 \times][\hat{\omega} \times] & \mathbf{0}_3 & \mathbf{I}_3 & -\hat{\mathbf{A}}[\mathbf{e}_1 \times] \\ 2\hat{\mathbf{A}}[\mathbf{e}_2 \times][\hat{\omega} \times] & \mathbf{0}_3 & \mathbf{I}_3 & -\hat{\mathbf{A}}[\mathbf{e}_2 \times] \end{bmatrix} \quad (16a)$$

$$\mathbf{H}\mathbf{F}^2 = \begin{bmatrix} -2\hat{\mathbf{A}}([\mathbf{e}_1 \times][\hat{\omega} \times]^2 + [\hat{\mathbf{a}} \times]) & \mathbf{0}_3 & \mathbf{0}_3 & \hat{\mathbf{A}}[\mathbf{e}_1 \times][\hat{\omega} \times] \\ -2\hat{\mathbf{A}}([\mathbf{e}_2 \times][\hat{\omega} \times]^2 + [\hat{\mathbf{a}} \times]) & \mathbf{0}_3 & \mathbf{0}_3 & \hat{\mathbf{A}}[\mathbf{e}_2 \times][\hat{\omega} \times] \end{bmatrix} \quad (16b)$$

$$\mathbf{H}\mathbf{F}^3 = \begin{bmatrix} 2\hat{\mathbf{A}}([\mathbf{e}_1 \times][\hat{\omega} \times]^3 + [\hat{\mathbf{a}} \times][\hat{\omega} \times]) & \mathbf{0}_3 & \mathbf{0}_3 & \cdots \\ 2\hat{\mathbf{A}}([\mathbf{e}_2 \times][\hat{\omega} \times]^3 + [\hat{\mathbf{a}} \times][\hat{\omega} \times]) & \mathbf{0}_3 & \mathbf{0}_3 & \cdots \\ \cdots & -\hat{\mathbf{A}}([\mathbf{e}_1 \times][\hat{\omega} \times]^2 + [\hat{\mathbf{a}} \times]) & & \\ \cdots & -\hat{\mathbf{A}}([\mathbf{e}_2 \times][\hat{\omega} \times]^2 + [\hat{\mathbf{a}} \times]) & & \end{bmatrix}. \quad (16c)$$

By inspection, one can show that  $\mathbf{H}\mathbf{F}^n$  with  $n > 0$  does not produce any additional independent rows, and therefore, it is sufficient to include only row matrices up to  $\mathbf{H}\mathbf{F}^3$  in the observability matrix (14). As shown in the Appendix, the observability matrix can be reduced to the following matrix by few elementary matrix row operations (MRO)

$$\mathcal{O} \xrightarrow{\text{MRO}} \mathcal{O}' = \begin{bmatrix} \mathbf{\Pi} & \mathbf{0}_3 & \mathbf{0}_3 & \mathbf{0}_3 \\ \times & \hat{\mathbf{A}}^T & \mathbf{0}_3 & \mathbf{0}_3 \\ \times & \mathbf{0}_3 & \hat{\mathbf{A}}^T & -[\mathbf{e}_1 \times] \\ \times & \mathbf{0}_3 & \mathbf{0}_3 & \mathbf{\Pi} \end{bmatrix} \quad (17)$$

where

$$\mathbf{\Pi} = \Delta\mathbf{e}\Delta\mathbf{e}^T[\hat{\mathbf{a}} \times] + [\hat{\mathbf{a}} \times] \quad (18)$$

and vector  $\Delta\mathbf{e} = \mathbf{e}_1 - \mathbf{e}_2$  is the antenna-to-antenna baseline vector. If matrix  $\mathbf{\Pi}$  is invertible, then the reduced observability matrix  $\mathcal{O}'$  can be transformed into a *block-triangular matrix* by premultiplying its fourth row by  $[\mathbf{e}_1 \times]\mathbf{\Pi}^{-1}$  and then adding it to the third row. In which case, the block-triangular matrix is full rank because all of its block diagonal matrices are invertible. Therefore, the full rankness of the reduced observability matrix rests on the invertibility of the square matrix  $\mathbf{\Pi}$ . In other words, if  $\mathbf{\Pi}$  is invertible, then system (6)–(13) is observable.

*Proposition 1:* If a line connecting the two GPS antennas is not parallel with the acceleration vector, then system (6)–(13a) is observable.

*Proof:* In a proof by contradiction, we show that  $\mathbf{\Pi} \in \mathbb{R}^{3 \times 3}$  must be a full-rank matrix if  $\hat{\mathbf{a}} \not\parallel \Delta\mathbf{e}$ , i.e., vectors  $\hat{\mathbf{a}}$  and  $\Delta\mathbf{e}$  are not parallel. If  $\mathbf{\Pi}$  is not full rank, then there must exist a nonzero vector  $\boldsymbol{\xi} \neq \mathbf{0}$  such that  $\mathbf{\Pi}\boldsymbol{\xi} = \mathbf{0}_{3 \times 1}$ , which can be written in this form

$$[\boldsymbol{\xi} \times] \Delta\mathbf{e} - \lambda \Delta\mathbf{e} = \mathbf{0}_{3 \times 1} \quad (19)$$

where

$$\lambda = \boldsymbol{\xi}^T(\Delta\mathbf{e} \times \hat{\mathbf{a}}). \quad (20)$$

Notice that (19) is the eigen equation of the skew-symmetric matrix  $[\boldsymbol{\xi} \times]$ . The only real eigenvalue solution of such skew-symmetric matrix is zero corresponding to eigenvector  $\boldsymbol{\xi}$ . Therefore, substituting  $\lambda = 0$  and  $\Delta\mathbf{e} = \boldsymbol{\xi}$  into (20) yields

$$\Delta\mathbf{e} \cdot (\Delta\mathbf{e} \times \hat{\mathbf{a}}) = 0. \quad (21)$$

The only possibility for nonzero vectors  $\Delta\mathbf{e}$  and  $\hat{\mathbf{a}}$  to satisfy the aforementioned identity is that the two vectors are parallel, which is a contradiction. Thus, it is not possible for  $\mathbf{\Pi}\boldsymbol{\xi} = \mathbf{0}$  to be true, meaning that matrix  $\mathbf{\Pi}$  is full rank and, hence, so is the observability matrix.

It is worth mentioning that the angle made by two vectors  $\Delta\mathbf{e}$  and  $\hat{\mathbf{a}}$  can be calculated by

$$\theta = \cos^{-1} \frac{|\Delta\mathbf{e} \cdot \hat{\mathbf{a}}|}{\|\Delta\mathbf{e}\| \|\hat{\mathbf{a}}\|}. \quad (22)$$

The aforementioned identity can be used in real time to check if the observability matrix is close to the ill condition  $\theta = 0$ . Clearly, if the vehicle remains stationary, i.e.,  $\dot{\mathbf{r}} = \ddot{\mathbf{r}} = \mathbf{0}_{3 \times 1}$ , the acceleration output  $\hat{\mathbf{a}}$  contains only the gravitational acceleration component. In this case, the pose estimator is simply observable if the antenna-to-antenna baseline is not parallel to the gravity vector.

2) *Single-GPS/IMU Integration*: Now, assume that only one GPS measurement is available, say GPS 1. Then, the sensitivity matrix becomes

$$\mathbf{H} = [-2\hat{\mathbf{A}}[\mathbf{e}_1 \times] \quad \mathbf{I}_3 \quad \mathbf{0}_3 \quad \mathbf{0}_3]. \quad (23)$$

Consequently, the first rows of the corresponding matrices in (16) constitute  $\mathbf{H}\mathbf{F}$  to  $\mathbf{H}\mathbf{F}^3$  matrices of the new observability matrix. By inspection, one can see that nonzero vector

$$\boldsymbol{\eta} = \begin{bmatrix} \hat{\mathbf{a}} \\ 2\hat{\mathbf{A}}(\mathbf{e}_1 \times \hat{\mathbf{a}}) \\ \mathbf{0}_{3 \times 1} \\ 2\hat{\omega} \times \hat{\mathbf{a}} \end{bmatrix}$$

lies in the null space of the new observability matrix  $\mathcal{O}$  because

$$\mathcal{O}\boldsymbol{\eta} = \mathbf{0}_{12 \times 1}. \quad (24)$$

This means that matrix  $\mathcal{O}$  is not full rank, and hence, system (23)–(13a) is not observable. In other words, at least two GPS antennas are required for the IMU/GPS integration system to be observable.

### III. ESTIMATOR DESIGN

The equivalent discrete-time model of the linearized system (13) is also required for the KF design. The state transition matrix over time interval  $t_\Delta$  is given by

$$\Phi(t_k + t_\Delta, t_k) = \Phi_k = e^{\mathbf{F}(t_k)t_\Delta}. \quad (25)$$

Then, using the sinusoidal solution of the matrix exponential of the cross product [28], [29], the state transition matrix  $\Phi_k(\tau) = \Phi(t_k + \tau, t_k)$  can be obtained by solving the matrix exponential problem (25) as

$$\Phi_k(\tau) = \begin{bmatrix} \Lambda_k(\tau) & \mathbf{0}_3 & \mathbf{0}_3 & \frac{1}{2}\Lambda'_k(\tau) \\ \mathbf{0}_3 & \mathbf{0}_3 & I_3\tau & \mathbf{0}_3 \\ -\hat{\mathbf{A}}_k[\hat{\mathbf{a}}_k \times] \Lambda'_k(\tau) & \mathbf{0}_3 & \mathbf{0}_3 & \mathbf{0}_3 \\ \mathbf{0}_3 & \mathbf{0}_3 & \mathbf{0}_3 & I_3 \end{bmatrix}$$

where the submatrices of the earlier matrix are given by

$$\begin{aligned} \Lambda_k(\tau) &= I_3 - \frac{\sin \|\hat{\omega}_k\| \tau}{\|\hat{\omega}_k\|} [\hat{\omega}_k \times] + \frac{1 - \cos \|\hat{\omega}_k\| \tau}{\|\hat{\omega}_k\|^2} [\hat{\omega}_k \times]^2 \\ \Lambda'_k(\tau) &= I_3 \tau + \frac{\cos \|\hat{\omega}_k\| \tau - 1}{\|\hat{\omega}_k\|^2} [\hat{\omega}_k \times] \\ &\quad + \frac{\|\hat{\omega}_k\| \tau - \sin \|\hat{\omega}_k\| \tau}{\|\hat{\omega}_k\|^3} [\hat{\omega}_k \times]^2. \end{aligned}$$

The IMU noise constitutes the continuous process noise of the entire system with covariance

$$E[\mathbf{w} \mathbf{w}^T] = \Sigma_{\text{imu}} = \text{diag}(\sigma_g^2 I_3, \sigma_a^2 I_3, \sigma_b^2 I_3).$$

The covariance matrix of the discrete-time process noise, which will be used by the KF, can be calculated by [34]

$$\mathbf{Q}_k = \int_0^{t_\Delta} \Phi_k(\tau) G \Sigma_{\text{imu}} G^T \Phi_k^T(\tau) d\tau. \quad (26)$$

Using the first-order approximation of the matrix exponential as  $\Phi_k(\tau) = e^{\mathbf{F}(t_k)\tau} \approx I_{12} + \mathbf{F}(t_k)\tau$  in (26) yields the covariance matrix in the following form:

$$\mathbf{Q}_k = \begin{bmatrix} \mathbf{Q}_{k_{11}} & \times & \times & \times \\ \mathbf{0}_3 & \mathbf{0}_3 & \times & \times \\ \mathbf{Q}_{k_{31}} & \mathbf{0}_3 & \mathbf{Q}_{k_{33}} & \times \\ \frac{1}{4}\sigma_b^2 t_\Delta^2 I_3 & \mathbf{0}_3 & \mathbf{0}_3 & \sigma_b^2 t_\Delta I_3 \end{bmatrix}$$

where

$$\begin{aligned} \mathbf{Q}_{k_{11}} &= \left( \frac{\sigma_b^2 t_\Delta^3}{12} + \frac{\sigma_g^2 t_\Delta}{6} \right) I_3 - \frac{\sigma_g^2 t_\Delta^3}{12} [\hat{\omega}_k \times]^2 \\ \mathbf{Q}_{k_{31}} &= \frac{\sigma_g^2 t_\Delta}{4} I_3 + \frac{\sigma_g^2 t_\Delta^2}{8} ([\hat{\omega}_k \times] - 2\hat{\mathbf{A}}_k[\hat{\mathbf{a}}_k \times]) \\ &\quad - \frac{\sigma_g^2 t_\Delta^3}{6} \hat{\mathbf{A}}_k[\hat{\mathbf{a}}_k \times][\hat{\omega}_k \times] \\ \mathbf{Q}_{k_{33}} &= \left( \sigma_a^2 + \frac{\sigma_g^2}{4} \right) t_\Delta I_3 - \frac{\sigma_g^2 t_\Delta^3}{3} \hat{\mathbf{A}}_k[\hat{\mathbf{a}}_k \times] \hat{\mathbf{A}}_k^T \\ &\quad + \frac{\sigma_g^2 t_\Delta^2}{4} ([\hat{\mathbf{a}}_k \times] \hat{\mathbf{A}}_k^T - \hat{\mathbf{A}}_k[\hat{\mathbf{a}}_k \times]). \end{aligned}$$

Now, one can design an EKF based on the derived models. Let us assume that the state vector is partitioned as  $\mathbf{x} = [\mathbf{q}_v^T \boldsymbol{\chi}^T]^T$ , where  $\boldsymbol{\chi} = [\mathbf{r}^T \dot{\mathbf{r}}^T \mathbf{b}^T]^T$  is the part of the state vector that excludes the quaternion. Then, the EKF-based observer for the associated linearized system (6) and (13) is given in two steps:

1) estimate propagation

$$\hat{\mathbf{x}}_{k/k-1} = \hat{\mathbf{x}}_{k-1} + \int_{t_k}^{t_k + t_\Delta} \mathbf{f}(\mathbf{x}, \mathbf{u}(\tau), \mathbf{0}) d\tau \quad (27a)$$

$$\mathbf{P}_{k/k-1} = \Phi_{k-1} \mathbf{P}_{k-1} \Phi_{k-1}^T + \mathbf{Q}_{k-1} \quad (27b)$$

and 2) estimate correction

$$\mathbf{K}_k = \mathbf{P}_{k/k-1} \mathbf{H}_k^T (\mathbf{H}_k \mathbf{P}_{k/k-1} \mathbf{H}_k^T + \mathbf{R}_k)^{-1} \quad (28a)$$

$$\Delta \hat{\mathbf{x}}_k = \mathbf{K}_k (\mathbf{z}_k - \mathbf{h}(\hat{\mathbf{x}}_{k/k-1})) \quad (28b)$$

$$\mathbf{P}_k = (I_{15} - \mathbf{K}_k \mathbf{H}_k) \mathbf{P}_{k/k-1} \quad (28c)$$

where  $\hat{\mathbf{x}}_{k/k-1}$  and  $\hat{\mathbf{x}}_k$  are *a priori* and *a posteriori* estimations of the state vector, and  $\mathbf{H}_k = \mathbf{H}(\hat{\mathbf{x}}_{k/k-1})$ . The state update follows the error-state update,  $\Delta \hat{\mathbf{x}} = [\Delta \hat{\mathbf{q}}_v^T \Delta \hat{\boldsymbol{\chi}}^T]^T$ , in the *innovation step* of the KF (28b). The update of “nonquaternion part” of the state vector, i.e.,  $\hat{\boldsymbol{\chi}}$ , can be easily obtained by adding the corresponding error to a priori estimation. However, quaternion update is more complicated because only the vector parts of the quaternion error  $\Delta \hat{\mathbf{q}}_{v_k}$  is given at every step time. Therefore, first, the scalar part of the quaternion variation should be computed from the corresponding vector part. Second, the quaternion update is computed using the quaternion multiplication rule. Consequently, the state update may proceed right after (28b) as

$$\begin{aligned} \hat{\boldsymbol{\chi}}_k &= \Delta \hat{\boldsymbol{\chi}}_k + \hat{\boldsymbol{\chi}}_{k/k-1} \\ \hat{\mathbf{q}}_k &= \begin{bmatrix} \Delta \hat{\mathbf{q}}_{v_k} \\ \sqrt{1 - \|\Delta \hat{\mathbf{q}}_{v_k}\|^2} \end{bmatrix} \otimes \hat{\mathbf{q}}_{k/k-1}. \end{aligned} \quad (29)$$

Covariance propagation in (27b) relies on the values of state transition matrix of the discrete-time system, which is linearized about the estimations of the states and the inputs at time  $t_{k-1}$ , i.e.,  $\Phi_{k-1} = \Phi(\hat{\mathbf{x}}_{k-1}, \hat{\mathbf{u}}_{k-1})$ . The sampling rate of IMU signals is usually higher than those of GPS signals. Therefore, the input estimation at every step time can be obtained from averaging of IMU signals between two consecutive GPS data acquisition in the interval  $t_k < t \leq t_k + t_\Delta$ . That is

$$\hat{\mathbf{u}}_{k-1} = \frac{1}{t_\Delta} \int_{t_{k-1}}^{t_{k-1} + t_\Delta} \mathbf{u}(\tau) d\tau.$$

Notice that incorporation of the decimated IMU signals in derivation of the state transmission matrix is a good approximation to be used only for covariance propagation. However, the position and orientation states are propagated separately by integration of the IMU inputs at the original sampling rate in the state propagation step (27a).

#### A. Estimation of the GPS Noise Covariance

Efficient implementation of the KF requires the statistical characteristics of the measurement and process noises. The covariances of the IMU noises can be treated as a constant

parameter, which can be either derived from the sensor specification or empirically tuned. However, the GPS measurement errors may vary from one point to the next, in which case the error depends on many factors such as satellite geometry, atmospheric condition, multipath areas, and shadow. Therefore, since the covariance matrix associated with the GPS noise is not known beforehand, it has to be estimated in the filter's internal model, so that the filter is “tuned” as much as possible [35].

In a noise-adaptive KF, the issue is that, in addition to the states, the covariance matrix of the measurement noise has to be estimated [35], [36]. The fundamental assumption on which the adaptive KF is based is that the innovation sequence can be effectively approximated as an ergodic process inside a sliding sampling window with length  $w$ . Let us define the residual error  $\varrho_k$ , which is obtained from the incoming GPS data information  $\mathbf{z}_k$  and the optimal *a posteriori* state estimates  $\hat{\mathbf{x}}_{k/k-1}$  according to

$$\varrho_k = \mathbf{z}_k - \mathbf{H}_k \hat{\mathbf{x}}_{k/k-1}. \quad (30)$$

The earlier equation can be equivalently written as

$$\varrho_k = \mathbf{H}_k (\mathbf{x}_k - \hat{\mathbf{x}}_{k/k-1}) + \mathbf{v}_k. \quad (31)$$

Taking variance of both sides of (31) gives

$$\mathbf{R}_k = \mathbf{S}_k - \mathbf{H}_k \mathbf{P}_{k/k-1} \mathbf{H}_k^T \quad \text{with} \quad \mathbf{S}_k = E[\varrho_k \varrho_k^T]. \quad (32)$$

The earlier equation can be used to estimate the measurement covariance matrix  $\hat{\mathbf{R}}_k$  from an ergodic approximation of the covariance of the zero-mean residual  $\varrho$  in the sliding sampling window with finite length  $w$ . That is,

$$\hat{\mathbf{S}}_k \approx \frac{1}{w} \sum_{i=k-w}^k \varrho_i \varrho_i^T \quad (33)$$

where  $w$  is chosen empirically to give some statistical smoothing [37]. The intuitive motion in choosing a finite window in the estimation of the innovation covariance matrix is that very past error data has to be discounted when being used for estimation of the current covariance. It is known that if the innovation sequence can be assumed to be essentially time invariant (ergodic) over the most recent  $w$  steps, then using (33) in (32) yields optimal estimation of the covariance matrix  $\hat{\mathbf{R}}_k$  in the sliding sampling window [37]. Then, the expression for recursive estimation of the covariance matrix is given by

$$\hat{\mathbf{S}}_k = \begin{cases} \frac{k-1}{k} \hat{\mathbf{S}}_{k-1} + \frac{1}{k} \varrho_k \varrho_k^T, & \text{if } k < w \\ \hat{\mathbf{S}}_{k-1} + \frac{1}{w} (\varrho_k \varrho_k^T - \varrho_{k-w} \varrho_{k-w}^T), & \text{otherwise.} \end{cases} \quad (34)$$

To summarize, the adaptive estimator for driftless pose estimation of a vehicle by fusing two RTK GPSs and IMU is schematically illustrated in Fig. 2.

### B. Initialization of KF

For the first iteration of the EKF, an adequate guess of the initial states is required. The initial position and orientation of the vehicle at  $t = 0$  s have to be carefully selected to keep the

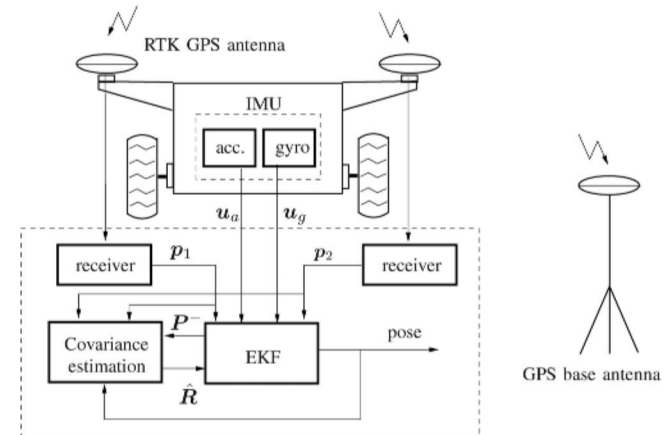


Fig. 2. Block diagram of the attitude determination and localization of a vehicle.

initial error in pose estimate as small as possible based on the information available from the measurements.

Let us form the following matrices:

$$\begin{aligned} \mathbf{M} &= [\Delta\mathbf{p}(0) \quad \mathbf{g} \quad \Delta\mathbf{p}(0) \times \mathbf{g}] \\ \mathbf{N} &= [\Delta\mathbf{e} \quad \hat{\mathbf{u}}_a(0) \quad \Delta\mathbf{e} \times \hat{\mathbf{u}}_a(0)] \end{aligned} \quad (35)$$

where  $\Delta\mathbf{p}(0) \triangleq \mathbf{p}_1(0) - \mathbf{p}_2(0)$  is the difference between the two GPS outputs at initial time  $t = 0$ . In view of (2), one can say that vector  $\Delta\mathbf{p}$  is the rotated version of vector  $\Delta\mathbf{e}$  if GPS noises are ignored. Moreover, in static case, where  $\dot{\mathbf{r}}(0) \equiv \ddot{\mathbf{r}}(0) \equiv \mathbf{0}$ , we can say vector  $\hat{\mathbf{u}}_a(0)$  is the rotated version of  $\mathbf{g}$  if the accelerometer noise is ignored too. Under these circumstances, the aforementioned two matrices are simply related by the rotation matrix as

$$\mathbf{M} = \mathbf{A}\mathbf{N}. \quad (36)$$

Matrices  $\mathbf{M}$  and  $\mathbf{N}$  are nonsingular as long as  $\mathbf{g}$  and  $\Delta\mathbf{p}(0)$  are not collinear, i.e., the line connecting the GPS antennas is not parallel to the gravity vector. Then, the rotation matrix can be obtained from matrix inversion as

$$\mathbf{A} = \mathbf{M}\mathbf{N}^{-1}. \quad (37)$$

Solution (37) yields a valid rotation matrix  $\mathbf{A}$  so that  $\mathbf{A}^T \mathbf{A} = \mathbf{I}_3$  only if there is no error in the column vectors of matrices (35). This may not be the case in practice, however, due to the IMU and GPS noises. To correct this problem, one may observe that all singular values of any orthogonal matrix must be one. This means that the singular value decomposition of the right-hand side of (37) yields

$$\mathbf{M}\mathbf{N}^{-1} = \mathbf{U}\Sigma\mathbf{V}^T$$

where  $\mathbf{U}$  and  $\mathbf{V}$  are orthogonal matrices and matrix  $\Sigma = \mathbf{I}_3 + \Delta_\Sigma$  is expected to be close to the identity matrix, i.e.,  $\|\Delta_\Sigma\| \ll 1$ . Therefore, by ignoring small matrix  $\Delta_\Sigma$ , a valid solution for the initial rotation matrix can be found as

$$\mathbf{A}(0) = \mathbf{U}\mathbf{V}^T \quad (38)$$

which, then, can be used to obtain the equivalent quaternion at  $t = 0$  s.



Fig. 3. CSA red rover with three RTK GPS antennas.

Now, with the initial guess of the rotation matrix in hand, one can obtain the initial guess of the position from (1) as

$$\mathbf{r}(0) = \frac{1}{2}(\mathbf{p}_1(0) + \mathbf{p}_2(0)) - \frac{1}{2}\mathbf{A}(0)(\mathbf{e}_1 + \mathbf{e}_2).$$

#### IV. EXPERIMENT

##### A. Driftless Attitude Determination Using Three GPS Antennas (Triangulation Method)

As will be discussed in the following, our vehicle is equipped with three RTK GPS antennas. Although only two GPSs are required by the adaptive KF, having three GPSs allowed us to measure the vehicle attitude purely from a kinematic relation through the triangulation method [23]. Since the three-GPS attitude determination method does not introduce any attitude drift, it can be used as a reference to investigate the long-term stability of GPS/IMU sensor fusion methods.

Assume that  $\mathbf{p}_3$  and  $\mathbf{e}_3$  denote the output of the third GPS and the location of its antenna on the vehicle, respectively. Also, denote  $\Delta\mathbf{p}' = \mathbf{p}_1 - \mathbf{p}_3$  and  $\Delta\mathbf{e}' = \mathbf{e}_1 - \mathbf{e}_3$ , and subsequently define matrices

$$\begin{aligned} \mathbf{Y} &= [\Delta\mathbf{p} \quad \Delta\mathbf{p}' \quad \Delta\mathbf{p} \times \Delta\mathbf{p}'] \\ \mathbf{Z} &= [\Delta\mathbf{e} \quad \Delta\mathbf{e}' \quad \Delta\mathbf{e} \times \Delta\mathbf{e}']. \end{aligned} \quad (39)$$

Then, identity

$$\mathbf{Y} = \mathbf{A}_\Delta \mathbf{Z} \quad (40)$$

holds in the absence of GPS measurement noise. Therefore, in a development similar to (35)–(38), one can calculate the rotation matrix from the earlier matrices. That is,

$$\mathbf{Y} \mathbf{Z}^{-1} = \mathbf{U} \Sigma \mathbf{V}^T, \quad \text{and} \quad \mathbf{A}_\Delta = \mathbf{U} \mathbf{V}^T.$$

##### B. Test Results

Fig. 3 shows the CSA red rover, which is equipped with three RTK GPS receivers along with satellite antennas and radio modems (model Promark3RTK from Magellan Navigation Inc., Santa Clara, CA) in addition to an IMU device from Crossbow

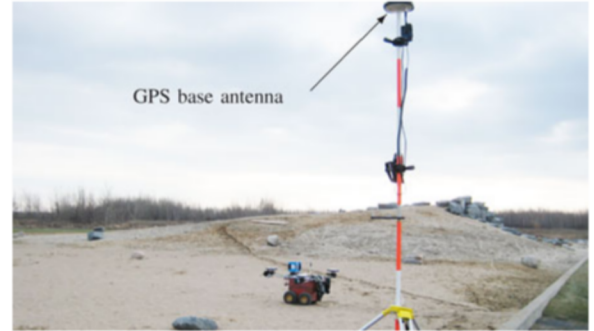


Fig. 4. Field test in the CSA MET.

TABLE I  
LOCATIONS OF GPS ANTENNAS EXPRESSED IN THE IMU FRAME

|       | $x$ (m) | $y$ (m) | $z$ (m) |
|-------|---------|---------|---------|
| $e_1$ | -0.452  | 0.604   | -0.252  |
| $e_2$ | -0.452  | -0.616  | -0.224  |
| $e_3$ | 0.427   | -0.003  | -0.249  |

Technology, Inc. (model IMU300). As explained in Section IV-A, only two GPSs are used for data fusion with IMU, while having three GPS systems allow us to measure the attitude in a driftless manner [38]–[40].

Experiments were conducted on the 30 m  $\times$  60 m Mars emulation terrain (MET) [41] of the CSA as shown in Fig. 4. The figure also shows the stationary GPS base antenna mounted on a surveying tripod located at a reference point of the CSA MET. The locations of the vehicle GPS antennas expressed in the vehicle frame are listed in Table I.

An operator sent a prescheduled sequence of primitive commands to the mobile robot—e.g., “move forward of a certain distance,” “rotate clockwise by 45°,” etc.—so that the robot follows a preplanned path going through some specified via points. Fig. 5 shows the 3-D path taken by the mobile robot passing through 14 via points. The GPS and IMU measurements are received at the rate of 1 and 20 Hz, respectively, and the corresponding time histories are plotted in Figs. 6 and 7. The variances of the IMU noise are set to  $\sigma_g = 2 \times 10^{-5}$  rad/s and  $\sigma_a = 0.25$  m/s<sup>2</sup>, while the covariance matrix of the baseline vector measurement from the two GPS data is estimated in the online fashion as illustrated in Fig. 8, where the size of the sliding window is chosen  $w = 5$ . It is apparent from the figure that the covariances are not constant, rather they fluctuate significantly over time. The angle made by the GPS antennas-to-antenna baseline and the acceleration vector is also calculated according to (22) and the time history is plotted in Fig. 9. It is clear from the graph that the angle is far from being zero indicating that the observability matrix always remains full rank.

In the first part of the experiment, the attitude estimations are obtained from the two cases of GPS/IMU data fusion configurations: 1) dual-GPS/IMU and 2) single-GPS/IMU. Subsequently, the estimations are compared with the attitudes calculated from the three-GPS method for investigating the long-term stability of the data fusion methods. Notice that the attitude obtained from the geometric three-GPS method is driftless, and therefore, it can be used as a reference to detect long-term drift in the

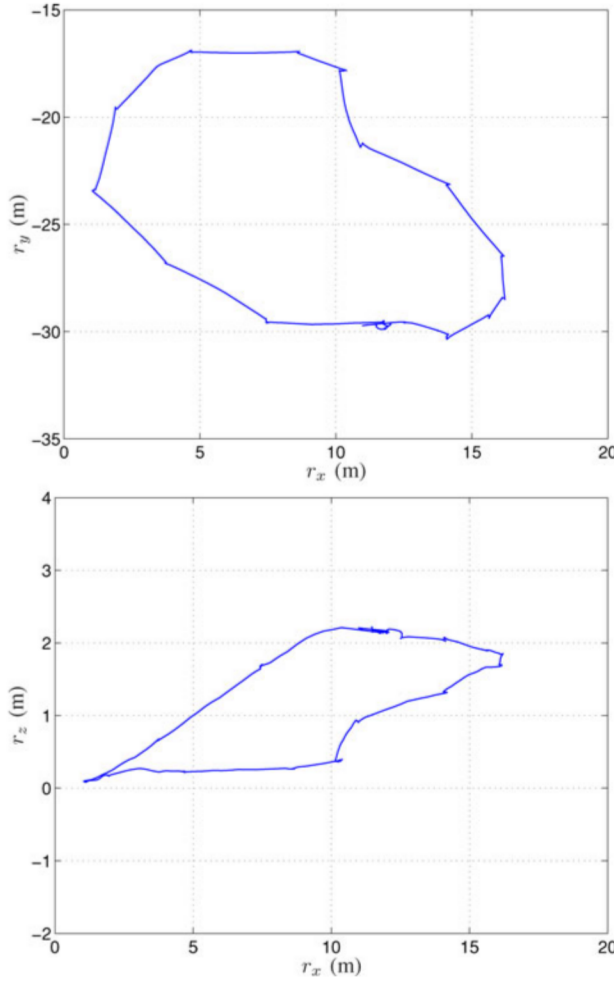


Fig. 5. Path taken by the mobile robot.

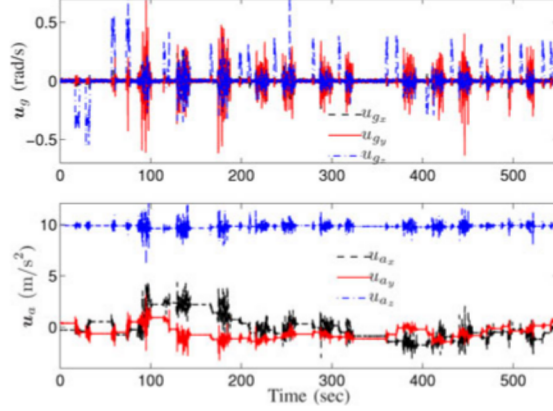


Fig. 6. Time histories of IMU outputs.

attitude estimation of the KF. Trajectories of the estimated vehicle attitude based on the dual-GPS/IMU and single-GPS/IMU sensor fusion configurations against the reference trajectories are illustrated in Fig. 10. The attitude estimate errors of the two GPS configurations with respect to the reference attitude are calculated in term of the Euler angles and the results are plotted in Fig. 11. It is evident from the graphs that the attitude estimate obtained from the dual-GPS/IMU integration does not

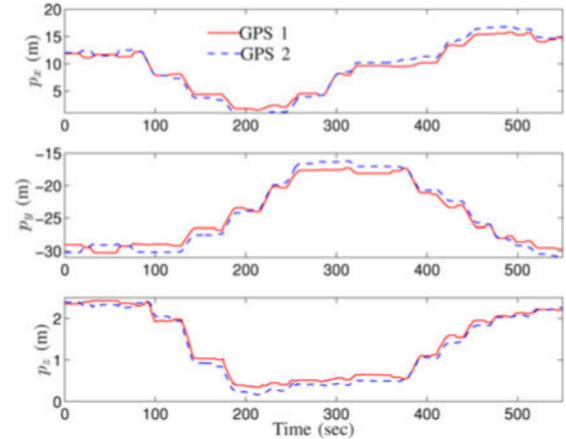


Fig. 7. RTK GPS outputs.

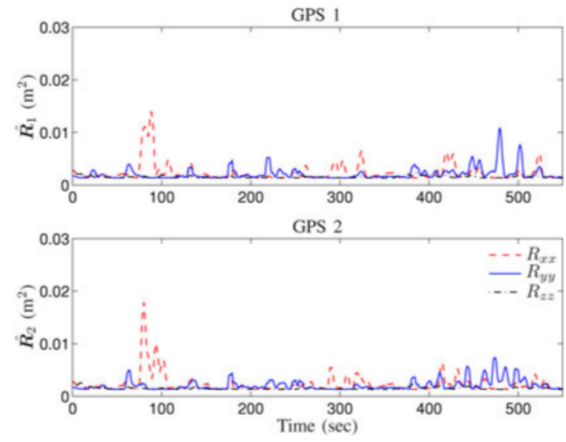


Fig. 8. Estimated covariances of the GPS measurement errors.

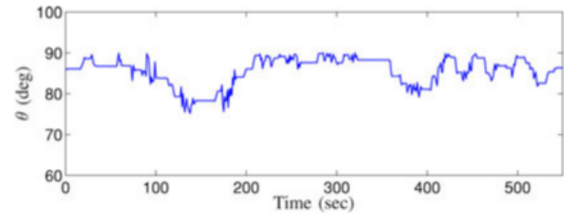


Fig. 9. Angle made by the vector of the measured acceleration and the line connecting two GPS antennas.

exhibit drift. However, there is significant drift in the yaw angle (also known as the bearing angle) estimation obtained from the single-GPS/IMU integration. This result was expected as the single-GPS/IMU integration method does not lead to an observable system necessary for convergence of the underlying KF. Fig. 12 illustrates the time history of the attitude errors<sup>1</sup> calculated by

$$\text{Attitude Error} = 2 \sin^{-1} \|\text{vec}(\hat{\mathbf{q}}^* \otimes \mathbf{q}_\Delta)\| \quad (41)$$

where quaternion  $\mathbf{q}_\Delta$  is equivalent to the rotation matrix (40), which is obtained from the triangulation method using three

<sup>1</sup>Here, quaternion  $\hat{\mathbf{q}} \otimes \mathbf{q}_\Delta^*$  represents the attitude error while scalar (41) is the corresponding rotation angle along the Euler axis.

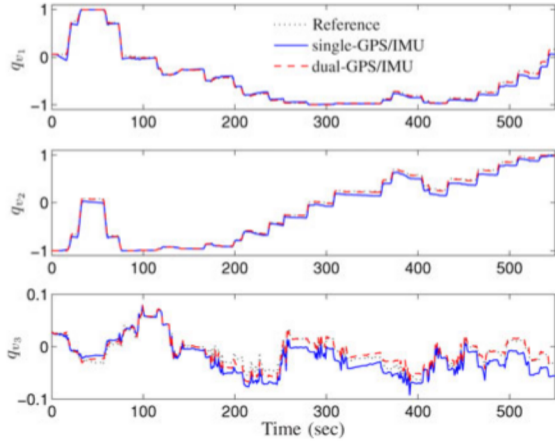


Fig. 10. Estimation of vehicle attitude.

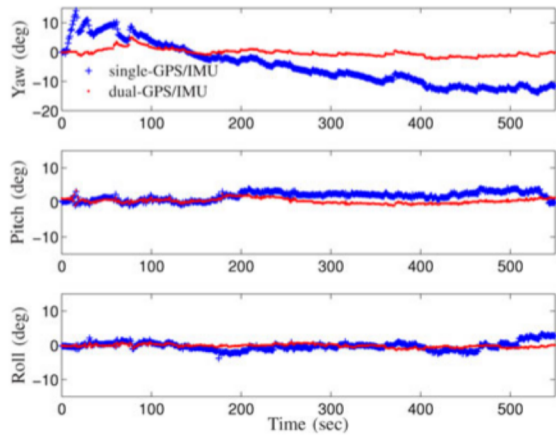


Fig. 11. Attitude errors represented by the Euler angles corresponding to the two GPS/IMU sensor fusion methods.

GPSs. The linear growth trend of the orientation error associated with single-GPS/IMU integration is quite obvious in the figures. On the other hand, it is evident from the figures that the attitude error associated with noise-adaptive KF does not grow with time. This clearly demonstrates that the attitude estimate from the dual-GPS/IMU integration does not exhibit any drift. Fig. 14 illustrates time histories of the gyro bias estimations obtained from the dual-GPS/IMU integration method.

The second objective of the experiment is to illustrate that IMU and GPS data fusion in the elaborate KF gives smooth estimations of the vehicle's attitude, position, and velocity compared to what can be obtained from multiple GPSs. Trajectories of the attitude and position estimates obtained from the KF data fusion method versus those calculated from GPS measurements are zoomed in Figs. 13 and 15. The figures clearly show the capability of the KF estimator to filter out the GPS noises. Motion control of mobile robots requires the velocity feedback in addition to the position feedback. To this end, the vehicle's velocity obtained from the differentiation of the GPS output is compared with the velocity estimate of the KF in Fig. 16. The graphs clearly illustrate that the GPS differentiation gives rise to the noise level, while the KF provides a smooth estimate of the velocity.

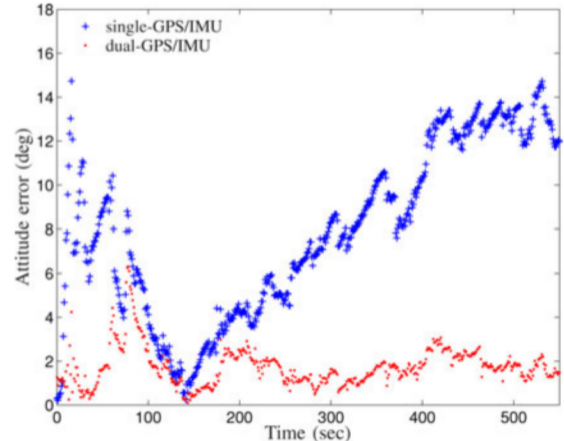


Fig. 12. Attitude errors corresponding to the two GPS/IMU sensor fusion methods.

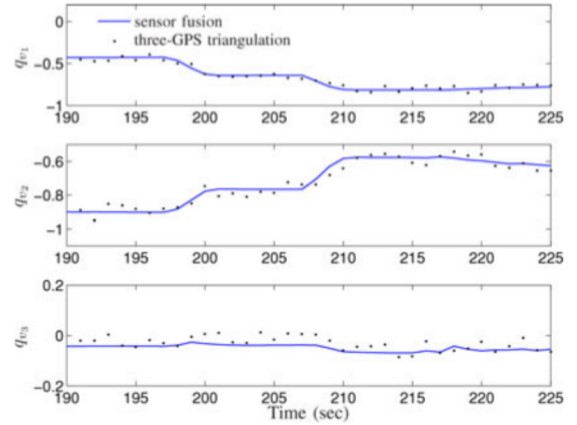


Fig. 13. Comparison between the attitude estimates obtained from the KF method and the three-GPS method.

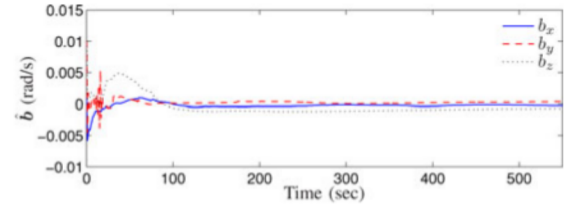


Fig. 14. Estimation of the gyro bias.

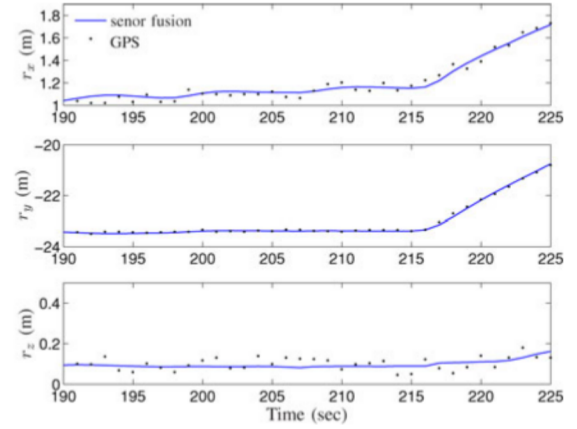


Fig. 15. Estimation of vehicle position.

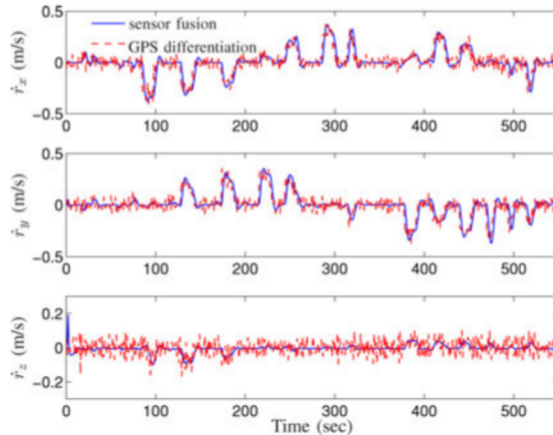


Fig. 16. Estimation of vehicle velocity.

## V. CONCLUSION

A method for 3-D attitude determination and positioning of mobile robots by fusing the information from a two RTK GPS units and an IMU in an adaptive KF has been developed. Examining the observability of different GPS/IMU integration systems has revealed that 1) the single-GPS/IMU integration system is not observable; and 2) the dual-GPS/IMU integration system is locally observable provided that the line connecting two GPS antennas is not parallel with the vector of the measured acceleration. Therefore, the dual-GPS/IMU integration method enabled the KF to compensate for the gyro drift in the data fusion process without using additional instrument for absolute orientation measurements, such as magnetic compass. Moreover, since the attitude estimation method did not rely on the heading angle measurement from the Doppler shift, it worked at low or zero speeds. In addition to the vehicle's position and orientation, the KF estimator was able to estimate the covariance of the GPS measurement noises in real time. This allowed to incorporate the GPS measurement heavily in the data fusion process only when GPS data became reliably available. A method for adequate initialization of the KF has been developed for fast and reliable convergence of the estimator. Test results have been presented demonstrating the long-term stability in pose estimation of a mobile robot moving in uneven terrain by integration of two RTK GPSs with IMU.

## APPENDIX

The following matrix:

$$\mathcal{O} \xrightarrow{\text{MRO}} \begin{bmatrix} [\Delta e \times] & \mathbf{0}_3 & \mathbf{0}_3 & \mathbf{0}_3 \\ \mathbf{e}_1^T [\hat{a} \times] & \mathbf{0}_{1 \times 3} & \mathbf{0}_{1 \times 3} & \mathbf{0}_{1 \times 3} \\ -\mathbf{e}_2^T [\hat{a} \times] & \mathbf{0}_{1 \times 3} & \mathbf{0}_{1 \times 3} & \mathbf{0}_{1 \times 3} \\ \times & \hat{\mathbf{A}}^T & \mathbf{0}_3 & \mathbf{0}_3 \\ \times & \mathbf{0} & \hat{\mathbf{A}}^T & -[\mathbf{e}_1 \times] \\ \times & \mathbf{0}_3 & \mathbf{0}_3 & [\Delta e \times] \\ \times & \mathbf{0}_{1 \times 3} & \mathbf{0}_{1 \times 3} & \mathbf{e}_1^T [\hat{a} \times] \\ \times & \mathbf{0}_{1 \times 3} & \mathbf{0}_{1 \times 3} & -\mathbf{e}_2^T [\hat{a} \times] \end{bmatrix}$$

can be constructed via the following elementary operations: the first row of the earlier matrix is obtained by premultiplying the first and second rows of  $\mathbf{H}$  in (6) by  $\hat{\mathbf{A}}^T$  and then subtracting the resultant row vectors. The second and third rows of the earlier matrix are obtained by premultiplying the first and second rows of  $\mathbf{HF}^2$  in (16b) by  $-\frac{1}{2}[\hat{\mathbf{A}}\mathbf{e}_1]^T$  and by  $\frac{1}{2}[\hat{\mathbf{A}}\mathbf{e}_2]^T$ , respectively. The fourth and fifth rows are obtained by premultiplying the first rows of  $\mathbf{H}$  in (6) and  $\mathbf{HF}$  in (16a) by  $\hat{\mathbf{A}}^T$ . The sixth row is obtained by premultiplying the first and second rows of  $\mathbf{HF}$  in (16a) by  $\hat{\mathbf{A}}^T$  and then subtracting the resultant row vectors. Finally, the seventh and eighth rows are obtained by premultiplying the first and second rows of  $\mathbf{HF}^3$  in (16c) by  $[\hat{\mathbf{A}}\mathbf{e}_1]^T$  and  $-[\hat{\mathbf{A}}\mathbf{e}_2]^T$ , respectively. Notice that the following identity

$$\mathbf{e}_i^T [\mathbf{e}_i \times] = \mathbf{0} \quad \forall i = 1, 2$$

was used in the earlier derivations. Adding the second and third rows of the earlier matrix and premultiplying the resultant row by  $\Delta e$  and repeating the operation for the seventh and eighth rows yields

$$\xrightarrow{\text{MRO}} \begin{bmatrix} [\Delta e \times] & \mathbf{0}_3 & \mathbf{0}_3 & \mathbf{0}_3 \\ \Delta e \Delta e^T [\hat{a} \times] & \mathbf{0}_3 & \mathbf{0}_3 & \mathbf{0}_3 \\ \times & \hat{\mathbf{A}}^T & \mathbf{0}_3 & \mathbf{0}_3 \\ \times & \mathbf{0}_3 & \hat{\mathbf{A}}^T & -[\mathbf{e}_1 \times] \\ \times & \mathbf{0}_3 & \mathbf{0}_3 & [\Delta e \times] \\ \times & \mathbf{0}_3 & \mathbf{0}_3 & \Delta e \Delta e^T [\hat{a} \times] \end{bmatrix}. \quad (42)$$

Now, one can readily show that by adding the first and second rows of matrix (42), and then, adding the fifth and sixth rows of matrix (42), the matrix is reduced to (17).

## REFERENCES

- [1] P. Oryschuk, A. Salerno, A. M. Al-Husseini, and J. Angeles, "Experimental validation of an underactuated two-wheeled mobile robot," *IEEE/ASME Trans. Mechatronics*, vol. 14, no. 2, pp. 252–257, Apr. 2009.
- [2] L. Kleeman, "Optimal estimation of position and heading for mobile robots using ultrasonic beacons and dead-reckoning," in *Proc. IEEE Int. Conf. Robot. Autom.*, Nice, France, May 1992, pp. 2582–2587.
- [3] J. Vaganay, M. J. Aldon, and A. Fournier, "Mobile robot attitude estimation by fusion of inertial data," in *Proc. IEEE Int. Conf. Robot. Autom.*, Atlanta, GA, May 1993, pp. 277–282.
- [4] Y. Fukui and E. Krotkov, "Dead reckoning for a lunar rover on uneven terrain," in *Proc. IEEE Int. Conf. Robot. Autom.*, Minneapolis, MN, Apr. 1996, pp. 411–416.
- [5] H. Chung, L. Ojeda, and J. Borenstein, "Accurate mobile robot dead-reckoning with a precision-calibrated fiber-optic gyroscope," *IEEE Trans. Robot. Autom.*, vol. 17, no. 1, pp. 80–84, Feb. 2001.
- [6] G. Dissanayake, S. Sukkarieh, E. Nebot, and H. Durrant-Whyte, "The aiding of a low-cost strapdown inertial measurement unit using vehicle model constraints for land vehicle applications," *IEEE Trans. Robot. Autom.*, vol. 17, no. 5, pp. 731–747, Oct. 2001.
- [7] J. Yi, J. Zhang, D. Song, and S. Jayasuriya, "IMU-based localization and slip estimation for skid-steered mobile robots," in *Proc. IEEE/RSJ Int. Conf. Intell. Robots Syst.*, San Diego, CA, Oct. 29–Nov. 2, 2007, pp. 2845–2850.
- [8] S. Lazarus, I. Ashokaraj, A. Tsourdos, R. Zbikowski, P. Silson, N. Aouf, and B. A. White, "Vehicle localization using sensors data fusion via integration of covariance intersection and interval analysis," *IEEE Sens. J.*, vol. 7, no. 9, pp. 1302–1314, Sep. 2007.
- [9] J. Yi, H. Wang, J. Zhang, D. Song, S. Jayasuriya, and J. Liu, "Kinematic modeling and analysis of skid-steered mobile robots with applications

- to low-cost inertial-measurement-unit-based motion estimation," *IEEE Trans. Robot.*, vol. 25, no. 5, pp. 1087–1097, Oct. 2009.
- [10] B. Barshan and H. F. Durrant-Whyte, "Inertial navigation systems for mobile robots," *IEEE Trans. Robot. Autom.*, vol. 11, no. 3, pp. 328–342, Jun. 1995.
- [11] M. Ahmadi and M. Buhler, "The ARL monopod II running robot: Control and energetics," in *Proc. IEEE Conf. Robot. Autom.*, Detroit, MI, May 1999, pp. 1689–1694.
- [12] A. Shaw and D. Barnes, "Landmark recognition for localisation and navigation of aerial vehicles," in *Proc. IEEE/RSJ Int. Conf. Intell. Robots Syst.*, Las Vegas, NV, Oct. 2003, pp. 42–47.
- [13] D. Bouvet and G. Garcia, "Improving the accuracy of dynamic localization systems using RTK GPS by identifying the GPS latency," in *Proc. IEEE Int. Conf. Robot. Autom.*, San Francisco, CA, Apr. 2000, pp. 2525–2530.
- [14] S. Panzieri, F. Pascucci, and G. Ulivi, "An outdoor navigation system using GPS and inertial platform," *IEEE/ASME Trans. Mechatronics*, vol. 7, no. 2, pp. 134–142, Jun. 2002.
- [15] R. Lenain, B. Thuilot, C. Cariou, and P. Martinet, "Adaptive control for car like vehicles guidance relying on RTK GPS: Rejection of sliding effects in agricultural applications," in *Proc. IEEE Int. Conf. Robot. Autom.*, Taipei, Taiwan, Sep. 2003, pp. 115–120.
- [16] H.-S. Choi, O.-D. Park, and H.-S. Kim, "Autonomous mobile robot using GPS," in *Proc. Int. Conf. Control Autom.*, Budapest, Hungary, Jun. 2005, pp. 858–862.
- [17] J. Huang and H.-S. Tan, "A low-order DGPS-based vehicle positioning system under urban environment," *IEEE/ASME Trans. Mechatronics*, vol. 11, no. 5, pp. 567–575, Oct. 2006.
- [18] J. I. Meguro, J. I. Takiguchi, Y. Amano, and T. Hashizume, "3D reconstruction using multibaseline omnidirectional motion stereo based on GPS/dead-reckoning compound navigation system," *Int. J. Robot. Res.*, vol. 26, no. 6, pp. 625–636, 2007.
- [19] C. B. Low and D. Wang, "Integrated estimation for wheeled mobile robot posture, velocities, and wheel skidding perturbations," in *Proc. IEEE Int. Conf. Robot. Autom.*, 2007, pp. 2355–2360.
- [20] C. B. Low and D. Wang, "GPS-based tracking control for a car-like wheeled mobile robot with skidding and slipping," *IEEE/ASME Trans. Mechatronics*, vol. 13, no. 4, pp. 480–484, Aug. 2008.
- [21] S. Shair, J. H. Chandler, V. J. Gonzalez-Villela, R. M. Parkin, and M. R. Jackson, "The use of aerial images and GPS for mobile robot waypoint navigation," *IEEE/ASME Trans. Mechatronics*, vol. 13, no. 6, pp. 692–699, Dec. 2008.
- [22] H. J. Woo, B. J. Yoon, B. G. Cho, and J. H. Kim, "Research into navigation algorithm for unmanned ground vehicle using real time kinematic (RTK)-GPS," in *Proc. IEEE ICCAS-SICE*, Fukuoka, Japan, Aug. 2009, pp. 2425–2428.
- [23] F. Aghili and A. Salerno, "Attitude determination and localization of mobile robots using two RTK GPSs and IMU," in *Proc. IEEE/RSJ Int. Conf. Intell. Robots Syst.*, St. Louis, MO, Oct. 2009, pp. 2045–2052.
- [24] E. Asadi and M. Bozorg, "A decentralized architecture for simultaneous localization and mapping," *IEEE/ASME Trans. Mechatronics*, vol. 14, no. 1, pp. 64–71, Feb. 2009.
- [25] L. Yang, Z. Guo, Y. Li, and C. Li, "Posture measurement and coordinated control of twin hoisting-girder transporters based on hybrid network and RTK-GPS," *IEEE/ASME Trans. Mechatronics*, vol. 14, no. 2, pp. 141–150, Apr. 2009.
- [26] F. Aghili and A. Salerno, "3-D localization of mobile robots and its observability analysis using a pair of RTK GPSs and an IMU," in *Proc. IEEE/ASME Int. Conf. Adv. Intell. Mechatronics*, Montreal, Canada, Jul. 2010, pp. 303–310.
- [27] T. Kang-Hua, W. Mei-Ping, and H. Xiao-Ping, "Multiple model Kalman filtering for MEMS-IMU/GPS integrated navigation," in *Proc. 2nd IEEE Conf. Ind. Electron. Appl.*, May 2007, pp. 2062–2066.
- [28] E. J. Lefferts, F. L. Markley, and M. D. Shuster, "Kalman filtering for spacecraft attitude estimation," *J. Guid. Control Dyn.*, vol. 5, no. 5, pp. 417–429, Sep./Oct. 1982.
- [29] M. E. Pittelkau, "Kalman filtering for spacecraft system alignment calibration," *AIAA J. Guid. Control Dyn.*, vol. 24, no. 6, pp. 1187–1195, Nov. 2001.
- [30] S. P. Won and F. Golnaraghi, "A triaxial accelerometer calibration method using a mathematical model," *IEEE Trans. Instrum. Meas.*, vol. 59, no. 8, pp. 2144–2153, Aug. 2010.
- [31] B. Southall, B. F. Buxton, and J. A. Marchant, "Controllability and observability: Tools for Kalman filter design," in *Proc. Brit. Mach. Vis. Conf.*, 1998, vol. 1, pp. 164–173.
- [32] D. Goshen Meskin and I. Y. Bar Itzhack, "Observability analysis of piecewise constant systems. I. theory," *IEEE Trans. Aerosp. Electron. Syst.*, vol. 28, no. 4, pp. 1056–1067, Oct. 1992.
- [33] M. Bryson and S. Sukkarieh, "Observability analysis and active control for airborne slam," *IEEE Trans. Aerosp. Electron. Syst.*, vol. 44, no. 1, pp. 261–280, Jan. 2008.
- [34] A. H. Jazwinski, *Stochastic Processes and Filtering Theory*. New York: Academic, 1970.
- [35] P. S. Maybeck, *Stochastic Models, Estimation, and Control*, vol. 2. New York: Academic, 1982.
- [36] C. K. Chui and G. Chen, *Kalman Filtering With Real-Time Applications*. Berlin, Germany: Springer-Verlag, pp. 113–115, 1998.
- [37] R. G. Brown and P. Y. C. Hwang, "The discrete Kalman filter, state-space modeling, and simulation," in *Introduction to Random Signals and Applied Kalman Filtering*. New York: Wiley, 1997, pp. 225–233.
- [38] Y. Bian, Ed., *Hard Target Penetrator End-Game Guidance*. DOD NAVY Grant, Topic: NAVY 97-116, 1997.
- [39] S. Winkler, M. Buschmann, L. Krüger, H.-W. Schulz, and P. Vörsmann, "AutoMAV—micro aerial vehicles for airport surveillance," in *Proc. IEEE TENCON*, Melbourne, Australia, Nov. 2005, pp. 1–6.
- [40] G. Giorgi, P. J. G. Teunissen, S. Verhagen, and P. J. Buist, "Improving the ambiguity success rate for attitude determination with the multivariate constrained LAMBDA method," in *Proc. IAG 2009 Conf. Geodesy Planet Earth*, Buenos Aires, Argentina, 2009.
- [41] I. Rekleitis, J.-L. Bedwani, S. Gemme, T. Lamarche, and E. Dupuis, "Terrain modelling for planetary exploration," in *Proc. 4th Can. Conf. Comput. Robot Vis.*, Montreal, QC, May 2007, pp. 243–249.



**Farhad Aghili** (SM'07) received the B.Sc. degree in mechanical engineering and the M.Sc. degree in biomedical engineering from Sharif University of Technology, Tehran, Iran, in 1988 and 1991, respectively, and the Ph.D. degree in mechanical engineering from McGill University, Montreal, QC, Canada, in February 1998.

During 1994–1997, he was a Research Engineer at MPB Technologies, Montreal. In January 1998, he joined the Canadian Space Agency. He is currently a scientist with the Space Exploration Division of the Canadian Space Agency (CSA), Saint-Hubert, QC, Canada. He has published more than 120 papers in journals and conference proceedings and is the author of seven patents and patent applications in the U.S. and Canada. His research interests include multibody dynamics, robotics, space robotics, vision systems, control systems, and mechatronics systems.

Dr. Aghili won the best paper award at the 2007 ASME/IEEE International Conference on Mechatronic and Embedded Systems and received the CSA Inventor and Innovator Certificate six times.



**Alessio Salerno** (M'01) received the Laurea degree from the University of Naples, Naples, Italy, in 2000, and the Ph.D. degree from McGill University, Montreal, QC, Canada, in 2006, both in mechanical engineering.

From 2006 to 2007, he was a Postdoctoral Research Scientist in the Department of Mechanical Engineering, Columbia University. Between 2008 and 2010, he was a Postdoctoral Fellow in the Robotics Group, Canadian Space Agency. In 2011, he joined the Control Software Group, Pratt & Whitney Canada, Longueuil, QC, Canada, as a Senior Mechanical Engineer. His research interests include dynamics and control of nonholonomic systems, mechatronics, mobile robotics, medical robotics, and space robotics.

Dr. Salerno is a member of the American Society of Mechanical Engineers (ASME).